ELSEVIER

Machine learning bridges local static structure with multiple properties in metallic glasses

Zhao Fan [1,*], Jun Ding [2], Evan Ma [1,*]

[1] Department of Materials Science and Engineering, Johns Hopkins University, Baltimore, MD 21218, United States
[2] Center for Advancing Materials Performance from the Nanoscale (CAMP-Nano), State Key Laboratory for Mechanical Behavior of Materials, Xi'an Jiaotong University, Xi'an 710049, PR China

A long-standing challenge in the metallic glass (MG) community has been how to quantitatively gauge the influence of the intricate local packing environment on the response (such as the propensity for atomic rearrangement) of the atomic configuration to external stimuli. Here we establish this structure–property relation by representing the complex amorphous structure using a single, flexibility-orientated structural quantity. This structural flexibility (*SF*) couples to a *bona fide* structural representation, the pair distribution function (PDF) of individual atoms, through a weighting function that reflects what matters in the static atomic configuration to dynamic responses. Machine learning is used, employing microscopic flexibility volume as the supervisory signal, to establish via direct regression an optimized weighting vector, which is proven robust for all quenching rates, deformation conditions, and different compositions in a given (e.g., Cu_xZr_{100-x}) alloy system. Subsequently, the *SF* is evaluated solely from the particle positions (PDF), for any structure variation, from the atomic scale up to sample average. Strong correlations are demonstrated between *SF* and a broad range of properties, including vibrational, diffusional, as well as elastic and plastic relaxation responses.

Introduction

The main objective of materials science is to establish concrete structure–property relations. The paradigm of "microstructure determines properties" has been very successful in explaining and predicting the behavior of conventional alloys. This is because these alloys are crystals, containing a plethora of property-controlling microstructural features, such as grains, precipitates, interfaces, dislocations, twins and stacking faults, etc., which can all be routinely identified under a microscope and judiciously manipulated during alloy processing [1]. The plastic flow, for example, is carried by well-defined dislocations and can be quantitatively explained by the evolution of these defects [2]. As a result, many predictive structure–property laws have been established, such as the Taylor hardening law based on dislocation density [3] and the Hall–Petch relationship for grain boundary strengthening [4,5].

In contrast, amorphous solids such as metallic glasses (MGs) present no discernible microstructure, invariably displaying a maze-like pattern when examined under a high-resolution transmission electron microscope. In other words, atoms adopt varying local atomic packing configurations and are all potential defects to various degrees. In terms of mechanical rigidity, MGs are more flexible than their crystalline counterparts: an MG typically exhibits a shear modulus ~30% lower [6], with considerable spatial heterogeneity even in a given sample [7,8]. The plastic susceptibility is variable as well, as nanometer-sized local regions respond to externally applied stresses to various extent [9–17]. The wide spectrum of local structures in an MG, i.e., the diverse short-range structures and their medium-range correlations, as well as the subtle differences between similar local configurations, makes it difficult to identify structural "defects"

* Corresponding authors.
E-mail addresses: Fan, Z. (zfan7@jhu.edu), Ma, E. (ema@jhu.edu).

 https://doi.org/10.1016/j.mattod.2020.05.021

responsible for the plastic events, even when the static structure (the coordinates or relative distribution of all atoms) is fully known. It remains unclear how to quantitatively bridge the local packing environment with its degree of likelihood for atomic rearrangements when exposed to external stimuli (such as applied stresses and temperature). As a result, explicit structure–property connections have been difficult to come by for MGs [18–37], let alone robust theoretical equations [38,39].

However, it has been generally believed that tell-tale signs about fertile sites, i.e., "defect"-like and responsive flow units or liquid-like regions, ought to be encoded in the structure of glasses. Research along this line of thinking found that a number of parameters, many of which are based on physical quantities but related to local packing structure, exhibit some degree of correlation with local properties. Examples include atomic-level stresses [40,41], configurational potential energy [25,42,43], local elastic modulus [44], soft modes (quasi-localized low-frequency vibration modes) [11,45], local yield stress [46,47], fictive temperature [48,49], local thermal energy [26] and thermal activation energy barrier [50,51]. However, each of these parameters is not directly determined by the spatial arrangement of atoms alone, but needs to be deduced from the knowledge of interparticle interactions through extensive computations. Some other indicators are more "structural", in the sense that they specify and focus on certain features of local atomic packing, such as free volume [27,52], short-range atomic packing order (coordination polyhedra) [9,10], correlated local order [28,53], degree of local five-fold symmetry (LFFS) [54], bond length deviation [55] and bond-orientational order [56]. But the correlation between any of these indicators and local properties is not sufficiently strong, partly because these short range order (SRO) indicators each provides only limited information to account for property variations. Unfortunately, the degree of order and coordination in the medium range (e.g., up to 2 nm) is difficult to decipher and rank for an amorphous solid [28,29]. Simultaneously accounting for several, or even "all of the above", facets of the structural ingredients pertaining to properties is an even more demanding proposition. Recently this challenge was paraphrased as an intellectual puzzle by the authors of a review on MGs [31]: atomic simulations at present, and experiments in future, can reach the point of mapping out the coordinates of each atom in an MG; but "knowing position of every atom; … then what to do with all that information?" In other words, while it is desirable to be able to predict properties solely from the (local) atomic configuration, current simplified/partial description of this environment does not correlate sufficiently well with properties, especially since the structural features influence the properties in a rather complex way (not black and white like in crystals, such as dislocations that carry all the action vs. perfect lattice).

In tackling this problem, recently we have come up with a new approach by introducing a structural indicator termed "flexibility volume", v_{flex} [57], which purposely encompasses both the static and dynamic local information. For atom i, $v_{flex,i}$ is defined as

$$v_{flex,i} = \langle r^2 \rangle_i \cdot a_i \quad (1)$$

where $\langle r^2 \rangle_i$ and a_i are the vibrational mean squared displacement (MSD) and interatomic distance [57], respectively. Here the MSD is used as a fiduciary detective that reports on how flexible a local environment would be upon excitation. We have established that v_{flex} quantitatively determines the shear modulus and exhibits strong correlations with multiple properties in MGs [57]. This robust relationship therefore solves a major part of the problem in the last paragraph. But v_{flex} has limitations in two aspects. First, v_{flex} is *not* just the static structure, which is the normally used and more accessible data from both simulation models and real MG samples. Instead, $\langle r^2 \rangle_i$ has to be mapped out to assess v_{flex} every time the sample changes, which is intractable in experimental work. Second, v_{flex} is difficult to define for MGs under high stress (pressure) or temperature, not to mention in liquid state and shear flow as the contribution of atomic diffusion cannot be easily separated out in those situations. So it is important and necessary to have a structural quantity which can be derived solely from static structural information and yet work as well as v_{flex}.

Objectives and general strategy

The goal of this work is to resolve the issue above. We now move the starting block to the static local structure in the MG. From this initial input we set out to establish a single quantity that represents the structure in terms of its adaptation to stimuli. We then use this new structural quantity, which will be termed structural flexibility (*SF*), to correlate with multiple properties, including vibrational and diffusional relaxation properties, as well as propensity for temperature- or stress-induced rearrangements in response to external stimuli (thermal, mechanical, etc.). These structure–property relations should also be applicable to (i.e., can be coarse-grained to) various levels/scales, all the way to a global average for the entire sample volume. Note that in the chain above, the initial input used in correlating with properties will be the static structure, and the key link is to "convert" this complex local atomic environment into a flexibility-centric single descriptor, *SF*. This conversion is made possible by machine-learning methods, and the translation takes advantage of the established structure parameter v_{flex}. This strategy will be illustrated in detail in the following, using results in the Cu_x-Zr_{100-x} model system.

Machine learning to link the static structure to structural flexibility

As stated above, in correlating with properties our mandate in this work is not to go from $v_{flex,i}$ as the structural input, but instead from square one, the static structure. But, $v_{flex,i}$ remains our vehicle to map the static structure to a new indicator, the *SF*. The $v_{flex,i}$ response of a local configuration is of course influenced by the atomic distribution surrounding the center atom i, but across a distance and in a complex way. This makes it challenging to simplify the inter-relation between the two, into a quantitative scaling. However, with the advent of the big data era, machine learning (ML) brings a new tool box that may help push the boundary of materials science. In fact, ML methods are particularly suited for establishing relations where simple theory has previously been intangible.

Before discussing step by step the structural representation, supervisory signal, and ML protocol in the sub-sections that follow, we first briefly comment on the recent use of ML to address

structure–property relations in glasses and supercooled liquids [13,14,58,59]. Cubuk et al. was the first to try ML on amorphous solids using L–J model glasses and jammed systems, showing that local radial, and bond-angle, distribution information can be used to separate atoms with high (versus low) susceptibility to displacement [13]. Wang and Jain used instead "interstice" distribution as the structural representation, in an effort to make the ML model less system-specific [59]. A separate attempt was made by Schoenholz et al. [58] at the correlation with dynamics: they used the magnitude of p_{hop} [60,61], as the supervisory signals in ML to separate out atoms with very large hopping rates. All these previous ML attempts, however, have left much to be desired for. First, they did training on a binary classification task but used the result as in a regression problem [62]. They had to rely on the distance to the separating hyperplane, or a class probability estimate, in describing the "softness" [58] (or quench-in softness [59]), to evaluate each atom's susceptibility to rearrangement. It would be more desirable to construct a structural flexibility quantity through direct ML regression, as will be done in this work. Second, the (local) softness defined was property-specific, i.e., it is trained on how "soft" the local environment is, with respect to a particular excitation. For example, the magnitude of none-affine squared displacement, D^2_{min}, for a given shearing was directly used as supervisory signals in training the ML model. The result is then already aligned with local plastic susceptibility under that specific loading condition. In other words, it is "trained on one specific behavior, tested and meant for recognizing that particular behavior for the most part". Every other property (such as hoping rate in diffusion) may often require a different ML model for the same MG structure. So for an MG alloy system we are missing a general ML product that can establish correlations with all essential properties. Third, the above suggests that when the MG structure is changed, e.g., via shear deformation in one loading condition, to predict the response under a different (loading) condition we may sometimes need to re-train the ML model. As a result, each property (e.g., D^2_{min}) may need to be evaluated *a priori* every time the sample changes, as the input variable for repeated training. This means that we cannot input static structural information only, but have to perform expensive atomistic computations accounting for all the interactions (much like directly using $v_{flex,i}$). These shortcomings point to a pressing need for advances in ML tactics, to reach higher and broader predictive power while requiring less non-structural input, which is our main objective put forward in the preceding paragraph.

Structural representation

As mentioned earlier, the properties of a local configuration are affected by the intricate and often collective physical and chemical interactions of atoms over a (at least medium-range) distance, in addition to the positions of these surrounding atoms in the local zone. So far, a single simple structure parameter falls short in correlating with properties. However, the spatial distribution of these atoms, i.e., where they are to begin with, is the most straightforward and accessible structural information that one would prefer to use, when it comes to correlating with properties. We therefore construct structure–property relations with this "local static structure" as the baseline input. Accordingly, we select the structural representation based on the widely used pair distribution function (PDF).

PDF represents the probability of finding atoms as a function of radial distance r from an average center atom [28]. The partial PDF (i.e., the element-specific PDF) for any α–β in the MG (such as Cu–Zr in our model system) is defined as [63]

$$g_{\alpha\beta}(r) = \frac{N}{4\pi r^2 \Delta r d N_\alpha N_\beta} \sum_{i=1}^{N_\alpha} \sum_{j=1}^{N_\beta} \delta(r - r_{ij}) \tag{2}$$

where d is the number density of atoms in the sample of N atoms, N_α and N_β are the number of atoms of species α and species β, respectively. r_{ij} is the distance between atom i (of α) and atom j (of β). Actually, the α–β partial PDF of a sample is an average of the partial PDF of each single atom, over all α atoms in the sample. Now we are dealing with local configuration around each individual atom, so we write the partial PDF of a *single* atom i as:

$$g(r)_{i,\beta} = \frac{1}{4\pi r^2 \Delta r d f_\beta} \sum_{j=1}^{N_\beta} \delta(r - r_{ij}) \tag{3}$$

where $f_\beta = \frac{N_\beta}{N}$ is the composition fraction of species β in a sample. In fact, $g(r)_{i,\beta}$ of a single atom i specifies the density of atoms (or number of atoms) of species β in the shell at distance r to the center atom i. Once the surrounding atoms across several neighboring shells within a cut-off distance are fixed, the local packing around the center atom i is defined. Thus the partial PDF of a single atom includes details on local environment across several shells, in addition to SRO, atomic volume (Ω) and coordination number (CN). The chemical order around a center atom is included as well, when all partial PDFs of the center atom are combined together. Therefore, we expect that the radial distribution of atoms surrounding atom i, embodied by all the partial PDFs, can adequately describe the local static structure, or at least closer to "all of the above" than the individual structural parameters mentioned earlier. This purely structural information will comprise a multi-dimensional vector $\boldsymbol{x}_i$ as our structural representation.

A new structural quantity

The next challenge is, as discussed earlier, how to convert the comprehensive static structure $\boldsymbol{x}_i$ into a more property-oriented and user-friendly structural quantity. We will need to i) re-cast the "structure" in terms of the degree of flexibility of the local configuration, and ii) do so in a way that simplifies this "structure" into a single quantity. As outlined earlier, this is achieved by defining a 'structural flexibility' (SF). The SF of atom i is

$$SF_i = \boldsymbol{\omega}^T \boldsymbol{x}_i \tag{4}$$

Here the superscript T represents the transpose of another vector ($\boldsymbol{\omega}$) that contains all the weighting factors reflecting the influence of the various aspects in $\boldsymbol{x}_i$ to flexibility. Mathematically, SF_i is the dot product of two column vectors, the static structural vector $\boldsymbol{x}_i$ and the weighting vector $\boldsymbol{\omega}$, resulting in a dimensionless scalar that can be utilized to rank property differences. Our next task is to solve for, via machine learning (ML), the complex $\boldsymbol{\omega}$ that cross-links $\boldsymbol{x}_i$ and SF_i.

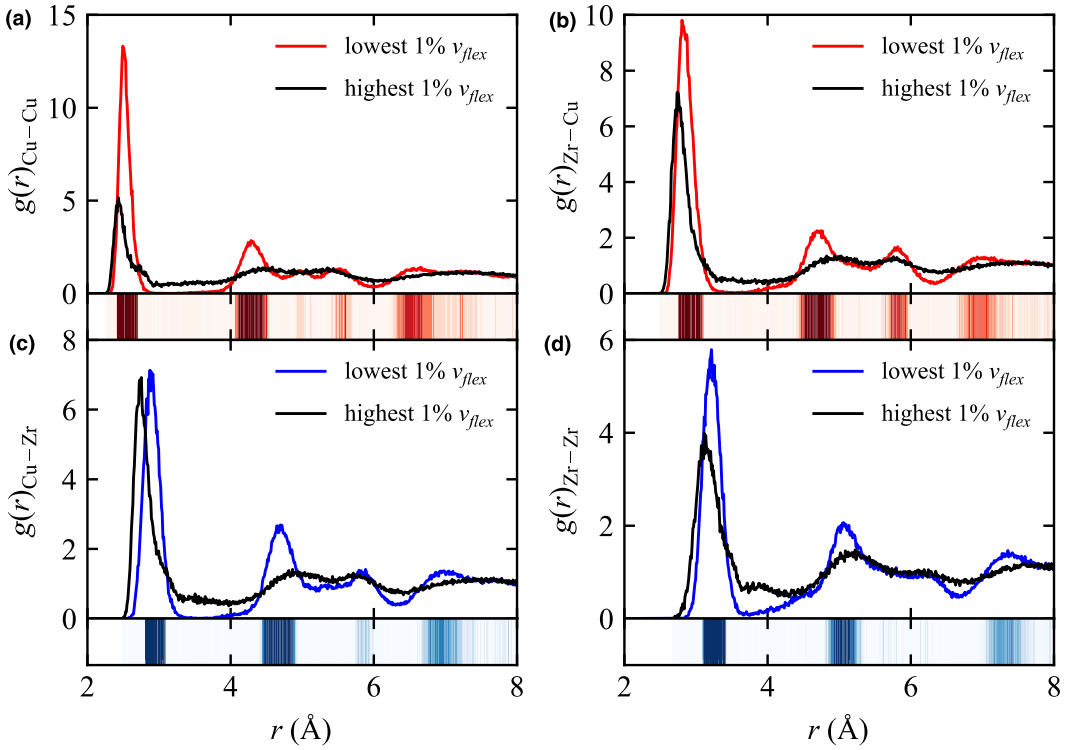

FIGURE 1

Partial pair distribution functions, $g(r)$, for Cu (a and c) and Zr (b and d) atoms with the lowest and the highest 1% $v_{flex,i}$ in a $Cu_{50}Zr_{50}$ MG. The model contains 1,024,000 atoms and quenched at an effective cooling rate of 1×10^{10} K/s. The upper and lower panels represent $g(r)_{\alpha\text{-Cu}}$ and $g(r)_{\alpha\text{-Zr}}$, respectively. The colored contour maps below $g(r)$ highlight the difference in $g(r)$ between atoms with the lowest and the highest 1% v_{flex}. The dark red (or blue) regions are where the radial density of Cu (or Zr) atoms in the most inflexible group is much higher than those belonging to the most flexible group.

Supervisory signal

The suitable supervisory signal to be used for ML, y_i, needs to reflect how flexible a local configuration is. v_{flex} comes in handy in this regard, as it contains dynamic information reflecting the wiggling propensity in the local environment while also depending on static local configuration to a large degree. Also importantly, $v_{flex,i}$ as a general flexibility indicator has strong correlation with multiple MG properties [57].

We now demonstrate that there is a strong inter-relation between local radial distribution and $v_{flex,i}$. The purpose of this exercise is to justify that by carrying out ML regression on these two, we can expect to land the ω that best transforms $\boldsymbol{x}_i$ into the flexibility-oriented *SF*. Our analysis can also shed light on what components/regions of the PDF really matters for flexibility. To this end, we sort the Cu (or Zr) atoms in our $Cu_{50}Zr_{50}$ MG model (see Methods) into 100 groups based on their $v_{flex,i}$ and computed the partial PDFs, $g(r)$, for each group. The partial PDFs of the 100 groups gradually evolve with increasing average v_{flex}; but for clarity, here we only contrast the extreme cases to gain some insight: in Fig. 1 we compare the $g(r)$ for the group of atoms having the lowest 1% v_{flex} (inflexible atoms) with that of the group of the highest 1% v_{flex} (flexible). We observe that (i) both the intensity and the position of the first peak are clearly different between these two groups of atoms; (ii) besides the first peak, there is no other pronounced peak on $g(r)$ for the most flexible atoms, while there are more than 3 visible peaks for the most inflexible atoms; (iii) for the inflexible atoms, almost no atoms fall in between the first and second peaks (wide trough with intensity close to 0). The colored contour maps below $g(r)$ show the difference in $g(r)$ between atoms with the lowest and the highest 1% v_{flex}. The dark red regions are where the radial density of Cu atoms is high, corresponding to the most inflexible group (dark blue regions for Zr). This is to be contrasted with the light red regions in between that correspond to the most flexible group (light blue for Zr). (iv) for Cu atoms, the first peak intensity ratio of Cu–Cu to Cu–Zr is greater than 1 for inflexible atoms, while that for flexible atoms is less than 1. For Zr center atoms, the first peak intensity ratio of Zr–Cu to Zr–Zr is greater than 1, deviating from the global composition ratio of Cu to Zr ($Cu_{50}Zr_{50}$). This indicates that chemical order also plays a role in v_{flex}, together with topological arrangement.

The findings in Fig. 1 suggest that, for atoms to be inflexible, they tend to require more surrounding Cu (Zr) atoms to appear in dark red (blue) regions, see the contour maps below $g(r)$ in Fig. 1, and less atoms to reside in other regions. In other words, the larger the ratio of neighboring atoms in the dark regions (peaks) to those in the light/bright regions (troughs), the more inflexible the central atom will be. Our results are consistent with, but much more convincing than, the hint mentioned in Ref. [13], where the authors contemplated that "soft" particles would have environments with fewer particles in their nearest neighbor shells but more in the troughs in between the shells.

Again, Fig. 1 helps to establish that the local flexibility ($v_{flex,i}$) is intimately connected with the local static structure ($\boldsymbol{x}_i$)around

an atom. The next question is "to what degree and how to quantify". This is where, and why, we bring in ML regression to secure the optimized $\boldsymbol{\omega}$. We reiterate that while $v_{flex,i}$ – property correlations have been established [57], that did not fully meet our objective. This is because $v_{flex,i}$ is not just static structural information, which is now our intended structural input to correlate with properties. In the meantime, also note that because of the universality and versatility of $v_{flex,i}$, a single ML model based on it would allow *SF* to correlate with multiple properties. In this context, $v_{flex,i}$ serves as an ideal ML supervisory signal.

The machine learning model

We now proceed to develop a concrete ML model to assess the flexibility of each atom from purely structural information embedded in $\boldsymbol{x}_i$. Now we will specify the exact forms of $\boldsymbol{x}_i, y_i$ and $\boldsymbol{\omega}$ to be used. Given that the $g(r)$ of a single atom is actually zero for the majority of the radial distance r and thus contains much redundant information, instead of using discrete PDF of each atom in the surrounding, we use Gaussian functions to weight the radial density at various distance $r \pm \sigma$ from the central atom i. The resultant structure function of each atom [13,58] is then

$$G_i^{\beta}(\bar{r}) = \sum_{j\in\beta,\bar{r}_{ij}\le\bar{r}_c} \exp\left(-\frac{(\bar{r}-\bar{r}_{ij})^2}{2\sigma^2}\right) \tag{5}$$

where $\bar{r}_{ij}$is the distance between the central atom i and the neighboring atom j of species β (Cu or Zr, here), within a cutoff $\bar{r}_c = 3.0$. Here $\bar{r}_{ij} = r_{ij}/r_p$, where r_p is the position of the first peak in the corresponding $g(r)$ of atoms with the lowest 1% $v_{flex,i}$ as shown in Fig. 1. The purpose of using this reduced distance here is to facilitate the check (later) if a ML model trained on one MG system can be transferred to other MG systems (nearly the same ML result can be achieved using real distance and a cutoff distance of 6.6 Å). For various $\bar{r}$ (within the range between 0.6 and $\bar{r}_c$, in increment of bin width $\sigma = 0.05$) and β, $G_i^{\beta}(\bar{r})$ measures the density of atoms of each species β at distance $\bar{r} \pm \sigma$ from the central atom i [58] and thus contains similar structural information as that in Eq. (3). A set of $G_i^{\beta}(\bar{r})$ at different distance $\bar{r}$ for species β can be viewed as Gaussian weighted partial radial distribution function for β atoms surrounding each reference atom i. All $G_i^{\beta}(\bar{r})$ sets for different β and a constant bias term $b = 1$ (the trainable parameter corresponding to the bias term is contained in the weight vector $\boldsymbol{\omega}$) are then assembled into a vector $\boldsymbol{x}_i$,

$$\boldsymbol{x}_i = [G_i^{\mathrm{Cu}}(\bar{r}_1), G_i^{\mathrm{Cu}}(\bar{r}_2), \cdots\cdots G_i^{\mathrm{Cu}}(\bar{r}_m), G_i^{\mathrm{Zr}}(\bar{r}_1), G_i^{\mathrm{Zr}}(\bar{r}_2), \cdots\cdots G_i^{\mathrm{Zr}}(\bar{r}_m), b = 1] \tag{6}$$

As noted earlier, this represents the static structure to be used to describe the local environment of atom i, for ML as well as in the structure–property relations we establish later.

We use $y_i = \ln(v_{flex,i})$ as the supervisory signal or target value. The use of natural logarithm makes training easier, when the distribution of the target value is close to a normal distribution. Through direct ML regression, we "fit" $\boldsymbol{x}_i$ and our actual y_i data to obtain the best weighting vector $\boldsymbol{\omega}$. In the context of Eq. (4), this means that the predicted dimensionless SF_i targets and approximates $\ln(v_{flex,i})$, keeping/reflecting the same ranking order as that of $v_{flex,i}$. The regression was carried out using L2-regularized L2-loss support vector regression (SVR), which is a linear algorithm, through minimizing the following loss function via adjusting the $\boldsymbol{\omega}$:

$$L = \frac{1}{2}\boldsymbol{\omega}^T\boldsymbol{\omega} + C\sum\nolimits_{i=1}^{l}\left[\max(0, |y_i - \boldsymbol{\omega}^T\boldsymbol{x}_i| - \varepsilon)\right]^2 \tag{7}$$

where C is a regularization parameter and $\varepsilon \ge 0$ is a parameter to specify the sensitiveness of the loss [64]. Again, with this weighting (scaling) function established through ML, we arrive at a single SF_i, which, being a scalar flexibility indicator, offers a power similar to $v_{flex,i}$ in correlating with various (other) properties in MGs. Moreover, now that we have finished feeding the $v_{flex,i}$ information into $\boldsymbol{\omega}$, from here on the *SF* can be computed solely from the $\boldsymbol{x}_i$. In other words, the static information about atomic positions is our initial, and from now on the only, structural input.

In the regression tasks, a high Pearson correlation coefficient ρ of 0.84 (and 0.82) between predicted and true values of y_i was achieved for the test set for Cu (and Zr). This quantitative relation is a further step of the qualitative connection between the local packing environment and flexibility observed in Fig. 1. As shown in SI, in classification task to separate out the least flexible atoms, our accuracy is as high as 98.4%. Because the data sets used in ML are sufficiently large, there is no over-fitting issue and the ML result is not sensitive to the regularization parameter C when C is larger than 1, as shown in Fig. S1. To ensure that our ML model can be applied across a large composition range in a MG system where glassy states can be obtained in experiments, our training and testing data sets are composed of atoms from Cu_xZr_{100-x} MGs at 9 compositions (x = 30, 35, . . ., 70, in step of 5). We have also confirmed that the ML model trained on the data set composed of atoms from a single composition has the same efficacy as that from 9 compositions, and can thus be transferred to other compositions in the same MG system. This is because the former data set was sufficiently large that it already covers the majority of the possible variations of local environment Cu (or Zr) atoms would see in the Cu–Zr system (see discussion in SI). As shown in Fig. S2, adjusting the value of $\bar{r}_c$ and σ in $G_i^{\beta}(\bar{r})$, or using neural network regression, did not yield visible improvement. Using interstice distribution [59] as structural representation lowered ρ slightly. Combining bond-angle structural functions with radial structural functions improved ρ only slightly, which is consistent with the observation in Ref. [58]. This further justifies the use of the local radial distribution alone, which is clear and simple in its physical meaning, as our structural representation ($\boldsymbol{x}_i$).

The high ρ achieved through SVR between $\boldsymbol{\omega}^T\boldsymbol{x}_i$ and $\ln(v_{flex,i})$ indicates a successful regression producing an optimized $\boldsymbol{\omega}$. As such, the evaluation of SF_i from here on no longer requires the computation of $v_{flex,i}$. Purely structural information embedded in $\boldsymbol{x}_i$ would suffice. In other words, once the machine-learned $\boldsymbol{\omega}$ is in hand, this same weighting vector $\boldsymbol{\omega}$ will be used as the designated machinery to convert static structural information into the "structure" in the context of flexibility, for this entire given MG alloy system. As can be seen from Equation (4), all that is needed to calculate SF_i is $\boldsymbol{x}_i$, which comes from the static atomic positions in a sample. We stress here that even though we have involved, through $v_{flex,i}$, the dynamics of atoms in the training to

construct ω, the latter is not a dynamical quantity but a structural one: it reflects the important aspects of the structural environment $\boldsymbol{x}_i$ that matter to the atomic flexibility in its dynamic response. The same can also be said for SF_i, which builds upon but goes beyond the static $\boldsymbol{x}_i$.

In what follows, we will demonstrate using the Cu_xZr_{100-x} MG models the ability of a single *SF* quantity to strongly correlate the (local) structure with multiple (at least five) microscopic/macroscopic properties, including shear modulus, soft vibrational modes, the boson peak, as well as the barriers for thermal activated rearrangements and stress-driven shear transformations. This represents a broad range of MG responses, from vibrational to diffusional to elastic/plastic relaxation events.

Correlations between *SF* and MG properties

Strong SF_i–$v_{flex,i}$ correlation for all MGs

As the ML model was trained and tested on $v_{flex,i}$, we first anticipate a strong correlation between the SF_i and $v_{flex,i}$, in other Cu–Zr MGs quenched at different cooling rates and at different compositions, those that were never involved in our ML training or testing. This is indeed seen in Fig. 2 for Cu atoms (and S3 for Zr). The ρ (displayed on these maps) between SF_i and $\ln(v_{flex,i})$ for Cu (Zr) atoms in these samples is almost the same as that in previous ML testing (shown in Fig. S4), confirming the generalizability of our ML models. The ρ is much higher than the corresponding ρ between Ω_i (or $LFFS_i$) and $\ln(v_{flex,i})$, shown in Figs. S5-8. As can be seen from Fig. 2 and Fig. S3, the largest scatter/deviation is mainly for atoms with extremely large $v_{flex,i}$ which are most sensitive to thermal fluctuation. If plotted against sample-averaged v_{flex}, the sample-averaged *SF* for Cu (or Zr) atoms scales linearly with it, as seen in Fig. 3a and b (or Fig. S9a and b). This is expected, as *SF* represents the flexibility-centric "structure", a dimensionless manifestation of v_{flex}. Fig. S10 shows that the sample-averaged *SF* for Cu (or Zr) atoms increases with increasing cooling rate or Zr concentration, which is the same trend that v_{flex} is known to exhibit [57].

Correlating structural flexibility with quasi-localized soft modes

The next demonstration is for the correlation between *SF* and the quasi-localized low-frequency vibrational modes [11,45]. The correlation between these two is expected to be strong, as the latter is known to correlate with the local atomic packing structure [45] and should correlate with v_{flex} [57], both being ingredients fed into *SF*. In Fig. 4a, we plot the distribution of the Cu atoms (the corresponding plot for Zr is in Fig. S11a) with the highest and the lowest 10% of SF_i (from 10 different $Cu_{50}Zr_{50}$ MGs) versus the participation fraction in soft modes, *p*, obtained by normal mode analysis (see details in methods section). As seen from Fig. 4a (and Fig. S11a), the maximum, mean and minimum values of *p* for Cu (Zr) atoms with the highest 10% SF_i are all much higher than corresponding values of Cu (Zr) atoms with the lowest 10% SF_i. To demonstrate that this correlation is strong, we contrast it with Fig. 4b (and Fig. S11b) where no obvious correlation is present with atomic volume Ω_i: the distributions for the highest and the lowest 10% of Ω_i overlap on top of each other. The correlation between *SF* and *p* also exists for Cu–Zr MGs with other compositions and processing history (cooling rates). We sorted Cu (Zr) atoms in each sample, based on increasing magnitude of SF_i, into bins each containing 10% of all the atoms and then computed the average *p* for the atoms in each bin. As seen from Fig. 4c and d (and Fig. S11c and d), there is a clear trend that the higher the *SF*, the larger the *p*.

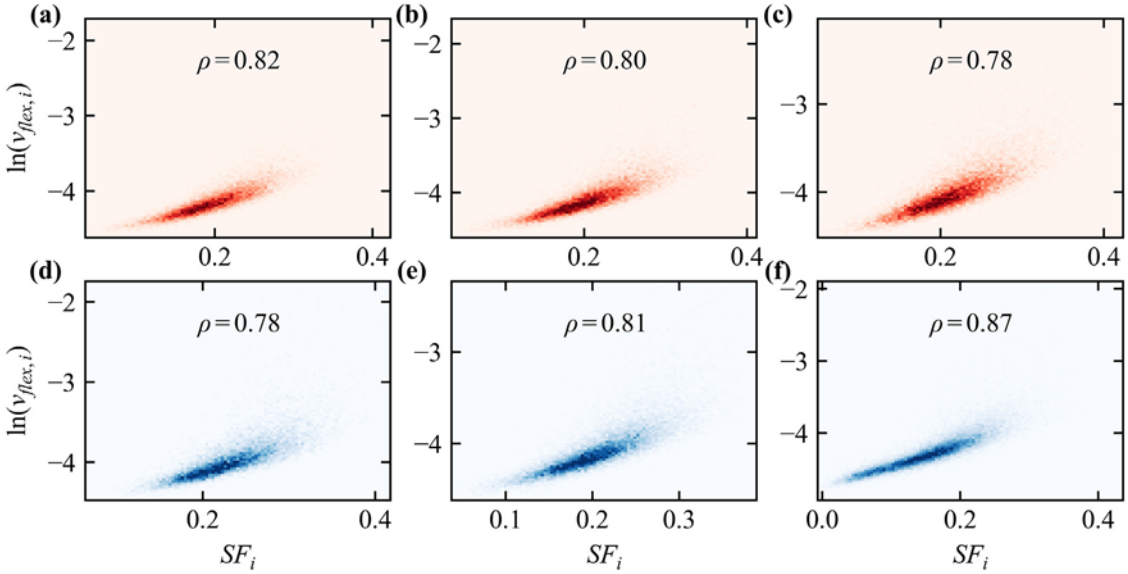

FIGURE 2

Correlation between structural flexibility SF_i and flexibility volume $v_{flex,i}$ of Cu atoms in Cu–Zr metallic glasses (MGs). The color in each plot scales with the density of atoms, dark (bright) corresponding to high (low) density of atoms. The Pearson correlation coefficient ρ between SF_i and $\ln(v_{flex,i})$ for each sample was shown in each figure. (a–c) Correspond to $Cu_{50}Zr_{50}$ MGs (31,250 atoms) quenched at cooling rates of 1×10^9, 1×10^{11} and 1×10^{13} K/s, respectively. (d–f) Correspond to $Cu_{30}Zr_{70}$, $Cu_{50}Zr_{50}$ and $Cu_{70}Zr_{30}$ MGs (32,000 atoms), respectively, quenched at the same effective cooling rate of 1×10^{10} K/s. The corresponding plots across the SF_i range of the Zr atoms are shown in Fig. S3.

Correlating structural flexibility with the boson peak

Boson peak (BP) is one of the universal features of glasses and typically ascribed to an excess vibrational density of states (VDOS). The origin of BP is still a matter of ongoing debate [65–71]. It has been shown that there is a strong correlation between the vibrational MSD and BP [67,68]. We thus expect the *SF* to have a strong correlation with BP. Fig. 5a shows the VDOS $g(\omega)$ of a $Cu_{50}Zr_{50}$MG (containing 1,024,000 atoms and quenched at 1×10^{10} K/s), which was obtained by the Fourier transform of velocity auto-correlation function [67,72] (see details in Methods). The BP can be observed easier by plotting reduced VDOS $g(\omega)/\omega^2$ over ω, as shown in Fig. 5b. To check the relation between *SF* and BP, we sorted all Cu (and separately Zr) atoms in the MG based on the magnitude of SF_i into groups each containing 2.5% of these atoms and then calculated the BP intensity (I_{BP}) contributed by the group. The I_{BP} of each group was plotted against group-averaged *SF*, as shown in Fig. 5c (S12a).

A strong correlation between BP intensity and *SF* is apparent in Fig. 5c (S12a). For comparison, we plotted in Fig. 5d (S12b) the BP intensity versus a recently introduced orientational order parameter, $\left|\overline{\Theta}_i^{BP}\right|$, which was shown to exhibit good correlation with BP [70]. The difference in I_{BP} between Cu (or Zr) atoms with the highest and the lowest 2.5% *SF* is 445 (370) μTHZ^{-3}, several times larger than the 119 (69) μTHZ^{-3} between the highest and the lowest 2.5% $\left|\overline{\Theta}_i^{BP}\right|$. This much better contrast is not a surprise, given that *SF* contains much more information while $\left|\overline{\Theta}_i^{BP}\right|$ is just a simple topological SRO parameter. The obvious correlation between *SF* and BP also holds for Cu–Zr MGs with different compositions and processing history, as shown in Fig. 3c and d (S9c and d).

The strong correlations so far between *SF* and vibrational behavior are somewhat expected, because vibrational displacements are directly involved in the $v_{flex,i}$ we feed as the target value

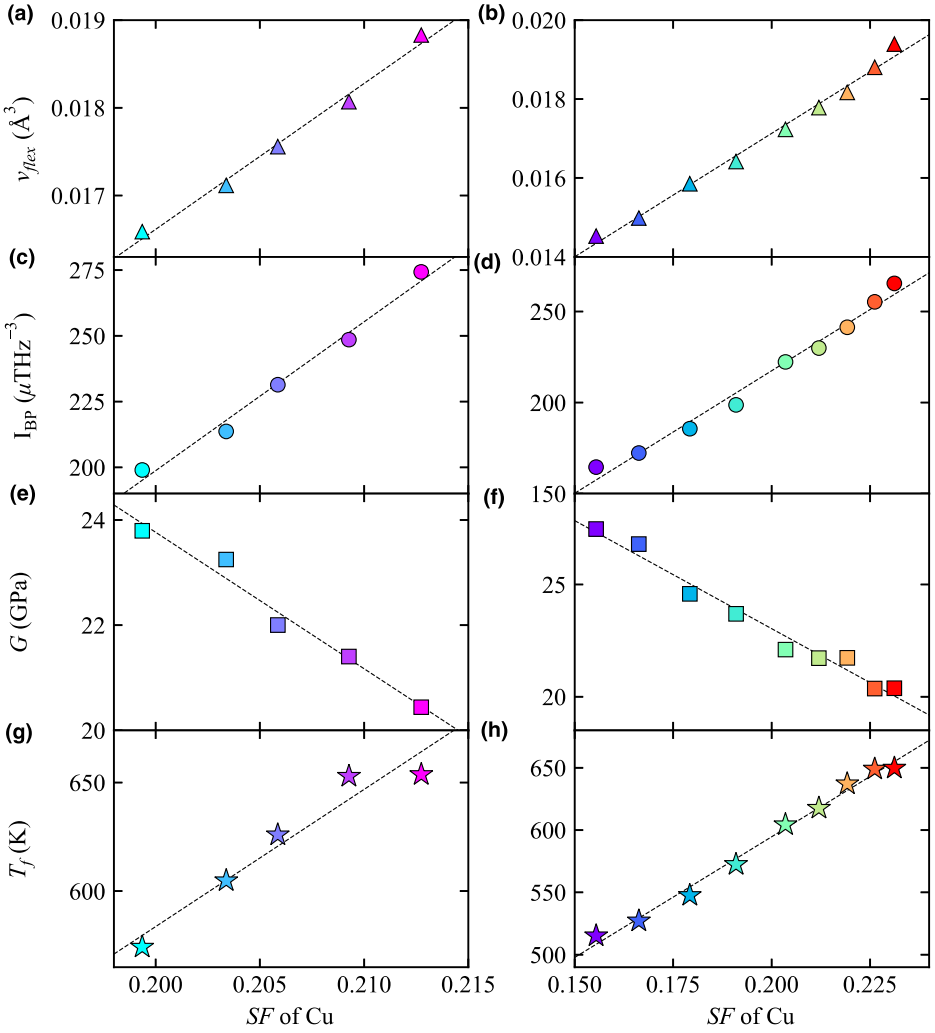

FIGURE 3

Correlation of structural flexibility *SF* averaged over all Cu atoms in a given MG with multiple macroscopic properties, for Cu–Zr MGs quenched at different cooling rates and at different compositions. The left column shows $Cu_{50}Zr_{50}$ MGs (31,250 atoms) quenched at cooling rates of 1×10^9, 1×10^{10}, 1×10^{11}, 1×10^{12} and 1×10^{13} K/s and the right column shows Cu_xZr_{100-x} MGs (where x = 30, 35, . . ., 70) (32,000 atoms) quenched at same effective cooling rate of 1×10^{10} K/s. The four rows, from top to bottom, are for four different sample-averaged properties for Cu atoms: v_{flex}, boson peak intensity I_{BP}, shear modulus G and fictive temperature T_f. The dash lines serve as a guide to the eye.

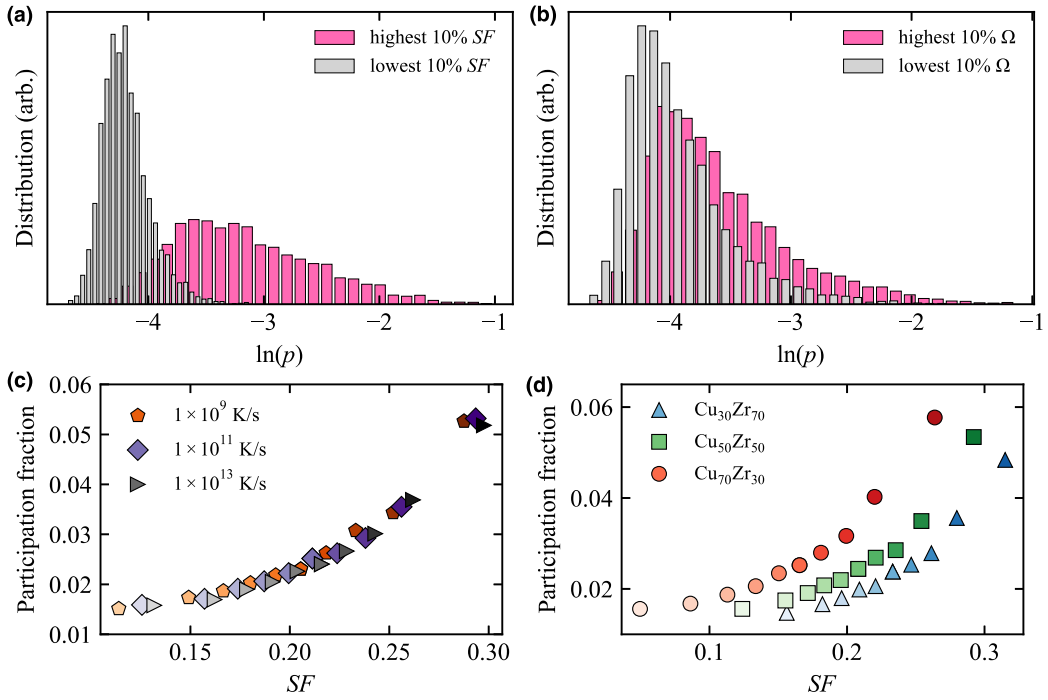

FIGURE 4

Structural flexibility correlates strongly with the participation in quasi-localized soft modes for Cu atoms. (a) Cu atoms with the highest 10% of SF_i show obviously higher participation fraction, p, than those with the lowest 10% SF_i. The same cannot be said when attempting to correlate p with (b) atomic volume Ω_i. The data are from 10 different $Cu_{50}Zr_{50}$ MGs each containing 10,000 atoms and quenched at the same cooling rate of 1×10^{10} K/s. (c) and (d) All the Cu atoms in a Cu–Zr MG are sorted based on their SF_i value into bins each containing 10% of the atoms. An average participation fraction (p) is then calculated for the atoms in each bin, and plotted to demonstrate the strong correlation with SF. The samples in (c) are $Cu_{50}Zr_{50}$ MGs each containing 10,000 atoms and quenched at three different cooling rates. The samples in (d) are Cu_xZr_{100-x} MGs (x = 30, 50 and 70) each containing 10,000 atoms and quenched at a cooling rate of 1×10^{10} K/s.

in working out the machine-learned ω. From here on, we move away from vibrational properties and establish correlations between the SF and several other key MG responses upon thermal and mechanical excitation. Note that in our approach relaxation events and shear transformations are not input variables in ML at all. Again, as we remarked earlier, we continue to project strong correlations across the board, because SF_i has been informed by $\nu_{flex,i}$, which is known to correlate well with (and therefore can "recognize") many MG properties [57].

Correlating structural flexibility with elastic constants

The shear modulus, G, a key parameter in MGs. Since G has been shown to be deterministically dependent on ν_{flex} for all MGs of different compositions and processing history [57], we expect a clear relation between SF and G. This is indeed observed in Fig. 3e and f (S9e and S9f), for the sample-average. As an example, Fig. 6 (S13) shows the spatial correlation between SF_i and local elastic moduli (C_{44}) of Cu (Zr) atoms in a slab having a thickness of 4.0 Å cut from a $Cu_{50}Z_{50}$ MG, where most of atoms with the lowest 5% SF_i (white circles) are located in regions with large (dark red region) local elastic moduli (C_{44}). Correspondingly, the highest 5% SF_i (black circles) coincide mostly with the small (light regions) C_{44} regions. Fig. S14 suggests a similar correlation for other Cu–Zr MGs at other compositions or with different cooling rates.

Correlating structural flexibility with stress-driven shear transformation

We next demonstrate the strong correlation of SF with stress-driven shear transformations. Athermal quasi-static shear (AQS) to a global strain of 5% (well below their yielding strain) was performed on Cu–Zr MG simulation models with various compositions and processing history, and then all Cu (or Zr) atoms in each sample are sorted based on their escalating magnitude of SF_i into bins each containing 10% of the total Cu (or Zr) atoms. Each bar chart in Fig. 7 (and S15 for Zr) shows the distribution of Cu atoms that have the top 5% non-affine squared displacement (D^2_{min}) [33] upon AQS. Here the vertical axis is the fraction of such Cu atoms, out of the total atoms in each bin. These histograms clearly show that the higher the SF_i of atoms, the larger the likelihood of participation in stress-driven shear transformation. The correlation is much stronger than those attempting to relate D^2_{min} with Ω_i or $LFFS_i$, as shown in Figs. S16–19. The contour maps in the row below each bar chart in Fig. 7 (S15) show a strong spatial correlation between SF_i and D^2_{min} on a slab of thickness of 4.0 Å arbitrarily cut from each sample.

One may notice that only <15% atoms out of those with the top 5% D^2_{min} are in the top 10% of SF_i; this is because shear transformation or D^2_{min} also depends on loading conditions, such as temperature, strain rate, loading orientation. For instance, the same local configuration can have very different D^2_{min} when the

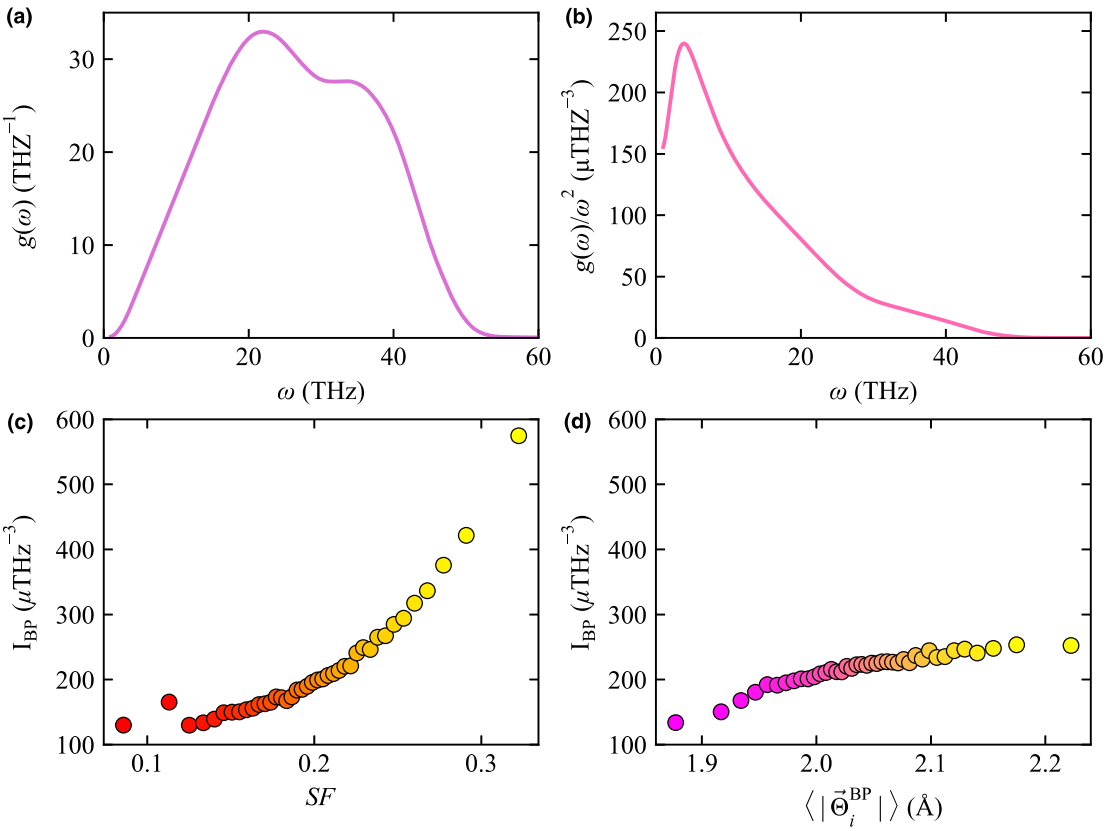

FIGURE 5

Correlation between structural flexibility and Boson peak. (a) and (b) show vibrational density of states (VDOS) $g(\omega)$ and reduced VDOS $g(\omega)/\omega^2$ of a $Cu_{50}Zr_{50}$ MG containing 1,024,000 atoms and quenched at effective cooling rate of 1×10^{10} K/s. In (c) and (d), all the Cu atoms in the MG are sorted based on SF_i and the length parameter $\left|\overline{\Theta}_i^{BP}\right|$, into bins each containing 2.5% of the atoms. The intensity of the boson peak, I_{BP}, is then calculated for each group of the atoms, and plotted against group-averaged SF and $\langle\left|\overline{\Theta}_i^{BP}\right|\rangle$.

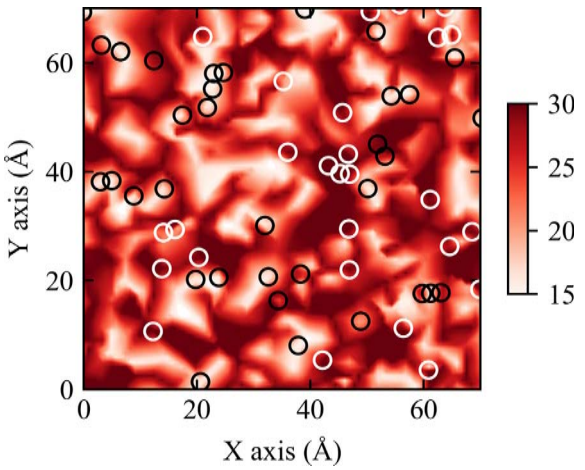

FIGURE 6

Spatial correlation between structural flexibility (SF_i) and local elastic moduli (C_{44}) for Cu atoms. The contoured map shows the spatial distribution of local elastic moduli (C_{44}) of Cu atoms in a slab having a thickness of 4.0 Å cut from a $Cu_{50}Z_{50}$ MG (31,250 atoms and quenched at a cooling rate of 1×10^9 K/s). The white (black) circles superimposed in the map mark the locations of Cu atoms with the lowest (highest) 5% SF_i.

shear is performed along different directions [33,47]. To take this into account, the D^2_{min} of a $Cu_{50}Zr_{50}$ MG was averaged over 4320 different loading conditions (see detail in caption of Fig. S20). As seen in Fig. S20, now when we examine Cu atoms having the top 5% average D^2_{min}, their fraction in the bin of the highest 10% SF_i almost doubles that in Fig. 7 (S15), with almost none residing in the bins for the lowest 20% SF_i. This convincingly establishes that SF_i correlates strongly with D^2_{min}.

Structural flexibility as an order parameter to monitor plastic flow in MGs

Four decades ago, Spaepen [27] developed strain rate equations to describe how deformation parameters (stress, temperature, etc.) affect the plastic flow behavior of MGs, employing free volume as the order parameter. However, as pointed out by Shi et al. [9,10] and Egami [73], free volume cannot be unambiguously defined for MGs, which are not hard sphere systems. Free volume is also not sensitive to specific atomic scale structures or the thermomechanical history of MGs. It is therefore desirable not to depend solely on the concept of free volume to model plastic flow for MGs. In the preceding section, we have demonstrated

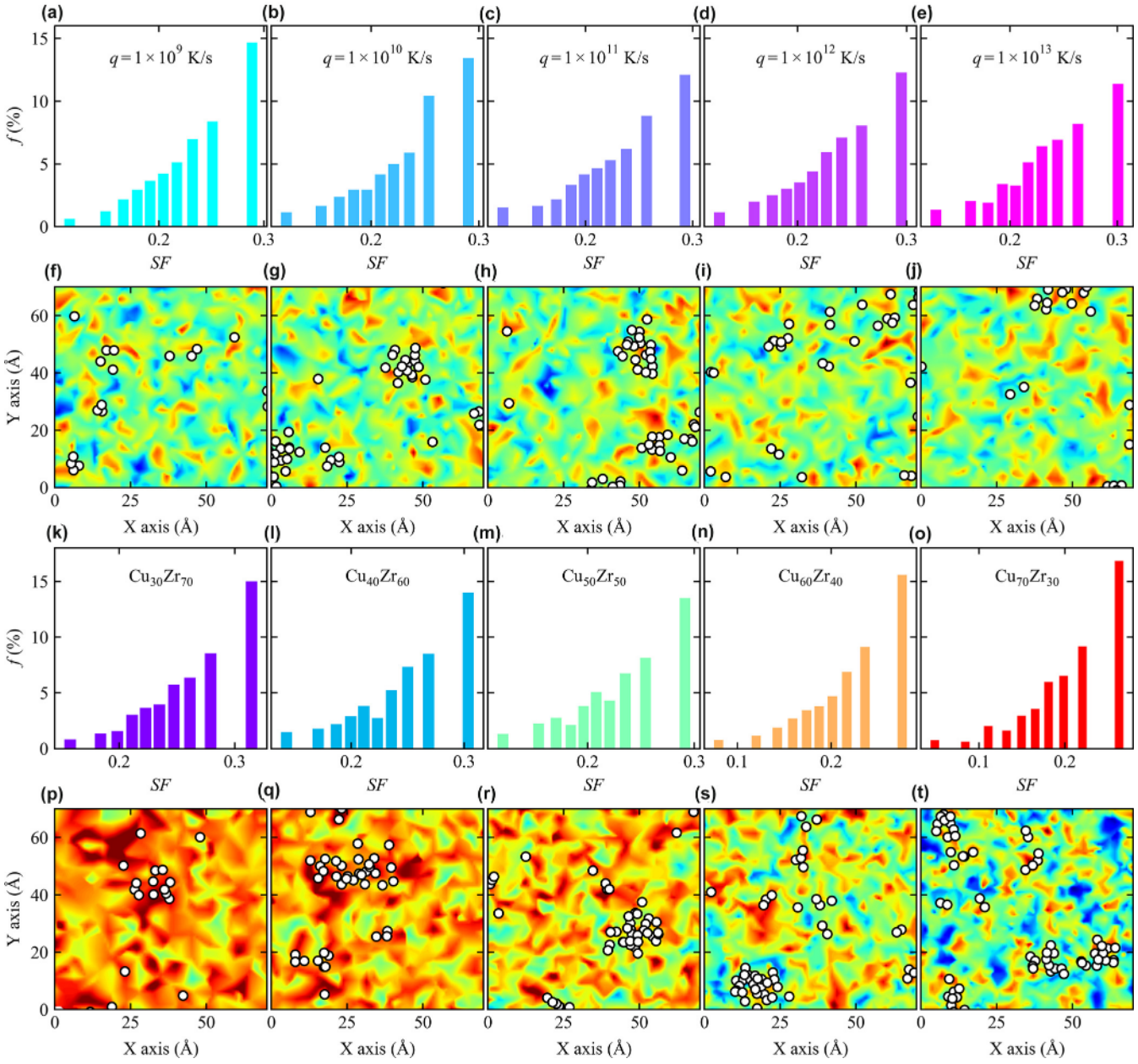

FIGURE 7

Strong correlation between structural flexibility (SF_i) and plastic susceptibility for Cu atoms in Cu–Zr MGs with various compositions and processing history. The simulation box was subjected to athermal quasistatic shear to a global strain of 5%. In the first row, each bar chart corresponds to one $Cu_{50}Zr_{50}$ MG which contains 31,250 atoms and was quenched at a specific cooling rate q labeled on top. In the third row, each bar chart corresponds to one Cu_xZr_{100-x} MG composition, for a model of 32,000 atoms quenched at the same effective cooling rate of 1×10^{10} K/s. Each bar chart shows the faction of Cu atoms with top 5% non-affine squared displacement (D^2_{min}), distributing the total number of these most-transformed Cu atoms into 10 bins each containing 10% of the total Cu atoms. Each contoured map below the bar chart shows the spatial distribution of SF_i of Cu atoms, in a slab having a thickness of 4.0 Å cut from the corresponding sample. Red (blue) corresponds to high (low) SF_i. White spots superimposed in the maps mark the locations of Cu atoms with top 5% D^2_{min}, mostly overlapping with the red regions. The corresponding charts and maps for Zr atoms are shown in Fig. S15.

that the machine-learned microscopic structural parameter, *SF*, strongly correlates with local plastic susceptibility in MGs. It is natural to ask if the evolution of *SF* during deformation can be used to predict the change of flow stress with increasing strain. We did AQS on Cu–Zr MGs with various compositions and processing history along *+xy* direction and monitored the evolution of stress, potential energy (*PE*) and system-averaged *SF* of both Cu and Zr atoms with strain. Fig. 8 confirms that the change of system-averaged *SF* correlates closely with both the flow stress and *PE* during deformation (note that volume is constant during AQS). Fig. S21 shows the distribution of D^2_{min} when a $Cu_{50}Zr_{50}$ MG (quenched at cooling rate of 1×10^9 K/s) was strained to 15%. To check if the change of *SF* could reflect the structural disordering in the region of shear localization (shear band), we divided the sample into 20 layers with equal thickness of ~4 Å parallel to the shear band plane (*xz* plane) and monitored the evolution of the average D^2_{min}, *SF*, and the number of atoms (*N*, which scales with the packing density and free volume content,

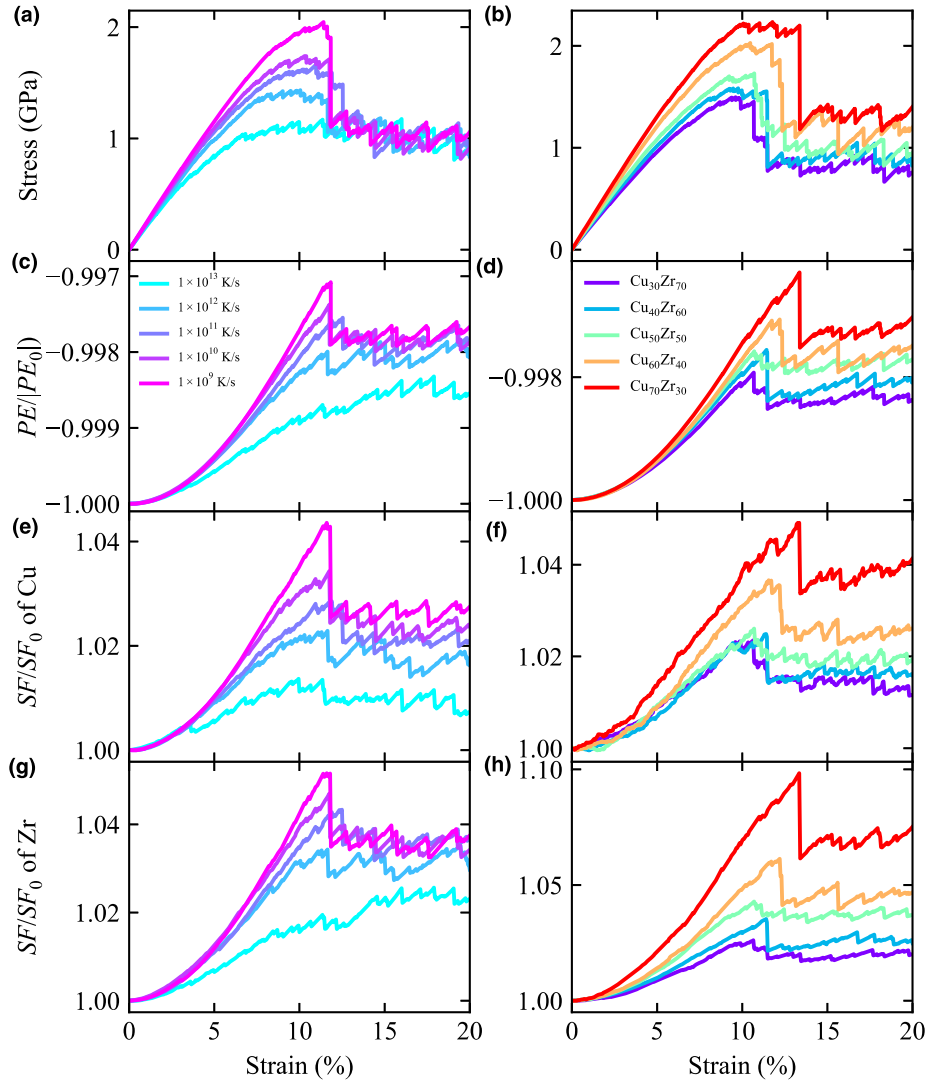

FIGURE 8

Evolution of stress (a and b), potential energy (*PE*) (c and d) and system-averaged *SF* of Cu (e and f) and Zr (g and h) with strain. The corresponding values at strain = 0, before athermal quasi-static shear (AQS), are used as the reference. Left column is for $Cu_{50}Zr_{50}$ MGs each containing 31,250 atoms and quenched over a range of cooling rates from 1×10^9 to 1×10^{13} K/s. Right column is for Cu_xZr_{100-x} MGs each containing 32,000 atoms and quenched at same effective cooling rate of 1×10^{10} K/s.

because the volume in each layer is the same) within each layer with strain. As can be seen from Fig. S22, when a single shear band forms at ~12% strain, both $D^2_{\min}$ and *SF* in all layers show a sudden change, and later deformation is mainly concentrated within the single shear band. The *SF* in the band is much higher than other regions. In contrast, the change of *N* in each layer seems random. As a specific example, Fig. S23a and b show the pronounced contrast of *SF* in and outside shear band when the sample was strained to 15%. These suggest that *SF* can serve as a single quantified order parameter to monitor the structural evolution upon straining and may possibly be incorporated into the formulation of plastic flow in MGs. In this regime, the *SF* is actually a more sensible parameter to use than v_{flex} to monitor the degree of structural flexibility of atoms. This is because, after global yielding most of the atoms are involved in the flow and the MSD rises drastically along with straining, containing not only contribution from atomic vibration but also contribution from shear-transformation assisted atomic diffusion. In contrast, *SF* is a simple quantity that requires only static structural information to calculate once an optimum ω is in hand, as stated earlier.

We note here that the current work is focused on monitoring local structure and predicting local shear transformation events, which are the basic unit of plastic activities. It is however not meant to cover all the mesoscopic or macroscopic plasticity behavior of MGs. When it comes to the ductility of a bulk MG under deformation, multiple length scales including the long-range soft spots [74] and shear band interactions need to be taken into account, but are beyond the scope of the present paper.

Correlating structural flexibility with thermally activated relaxation events

Since v_{flex} is known to have a good correlation with the activation energy barrier, ΔE, for thermally activated β processes including relaxation [57], which are related to glass transition, aging,

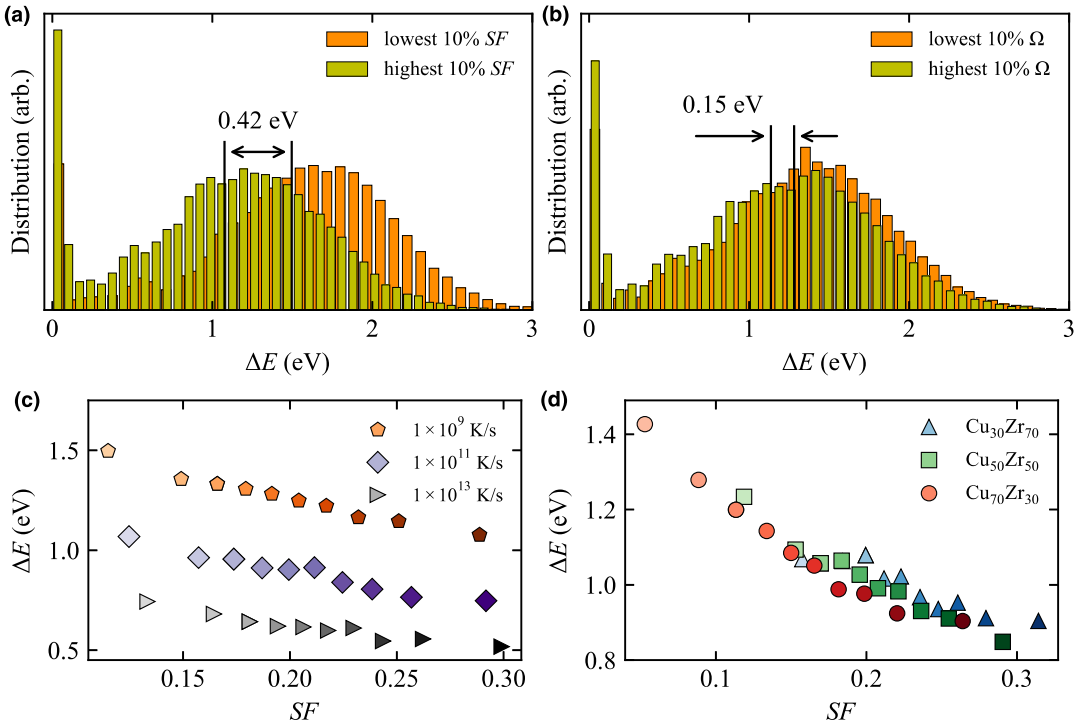

FIGURE 9

Correlation between structural flexibility and thermally activated relaxation events for Cu atoms. Distribution of thermally activation energy (ΔE) of Cu atoms in a $Cu_{50}Zr_{50}$MG (31,250 atoms and quenched at cooling rate of 1×10^9 K/s) characterized using ART nouveau. (a) Shows the two groups with the highest and lowest 10% of structural flexibility (SF_i), and (b) is for the two groups with the highest and lowest 10% of the values for the atomic volume (Ω_i). The difference in average ΔE between the two groups in the case of SF_i is 0.42 eV, much larger than 0.15 eV in the case of Ω_i. In (c) and (d), all the Cu atoms in each composition or cooling rate are sorted based on SF_i, into bins each containing 10% of the atoms. An average activation energy is then calculated for the atoms in each bin, and plotted to demonstrate the correlation with structural flexibility. In (c), all samples are $Cu_{50}Zr_{50}$MGs and the data for cooling rates of 1×10^{11} and 1×10^{13} K/s are from 5 samples each containing 2000 atoms while data for cooling rate of 1×10^9 K/s is from one sample containing 31,250 atoms. In (d), all samples are quenched at same effective cooling rate of 1×10^{10} K/s and the data for each composition are from 5 samples each containing 2000 atoms.

atomic hopping and other important properties in MGs, we also expect a strong correlation between *SF* and ΔE. We searched 30 relaxation events centered at each Cu (or Zr) atom in a $Cu_{50}Zr_{50}$ MG (31,250 atoms and quenched at 1×10^9 K/s) using the activation-relaxation technique (ART nouveau) [12,75,76] (see details in Methods). We then compared the distribution of ΔE of these events with the highest and the lowest 10% SF_i. As seen in Fig. 9a (Fig. S24a), there is a marked difference in average ΔE between the two groups, 0.42 (0.26) eV. In contrast, the distributions for atoms with the highest and the lowest 10% Ω_i almost overlap on top of each other, and the difference in average ΔE is much smaller, as shown in Fig. 9b (S24b). We also sorted Cu (Zr) atoms in Cu–Zr MGs with various cooling rates or compositions based on SF_i into bins each containing 10% of these atoms and calculated the average ΔE for each bin. All these samples show a clear correlation that the higher the group-average *SF*, the lower its average ΔE, as show in Fig. 9c and d (S24c and d).

In addition, fictive/effective temperature (T_f) is another way to represent the average structural state of glassy materials [48,49,51]. Previously, Liu et al. [51] showed that for MGs at a fixed composition, the system-average ΔE changes monotonically with cooling rate and thus correlates with T_f. Such a trend is also seen for our $Cu_{50}Zr_{50}$, as shown in Fig. S25a, but absent for different compositions (Fig. S25b). Thus, a correlation between the system-average *SF* and T_f is expected. This is indeed observed, as shown in Fig. 3g and h (S9g and h).

Conclusion

Our results above bring about several advances over previous efforts to establish structure–property relations in MGs, including recent attempts employing ML. First of all, to probe into the structural origin of MG behavior, we have taken the perspective that the (local) properties should be controlled by a more property-oriented and flexibility-centric "structure" that combines comprehensive structural attributes including where and how the surrounding atoms are distributed spatially, their (short-to-medium-range) interactions, and the dynamic wiggle room indicative of the collective agitation of the (local) atomic configuration. A sensible approach is to cover all these grounds, absorbing and summarizing them into a "cover-all" but simple structural quantity. We did so with *SF*. Second, this SF_i quantity is still based on $\boldsymbol{x}_i$, which is about the atomic coordinates across several neighboring shells embedded in the partial radial (atomic) density distributions. In other words, our approach allows the "structure" in the structure–property relations to be assessed from static packing environment, $\boldsymbol{x}_i$. Third, because $\boldsymbol{x}_i$ is too complicated for a quantifiable correlation with properties,

this initial structural input is translated/converted into a SF_i, which is informed by how responsive the atomic configuration would be upon excitation. Here through ML we have taken advantage of our recently established atomic $v_{flex,i}$ as the informant. The fourth advance is that we have used ML regression to link the complex local radial density distribution ($\boldsymbol{x}_i$) and flexibility. This direct linear regression gives us an optimized $\boldsymbol{\omega}$ with high Pearson correlation coefficient. The *SF* combining the ($\boldsymbol{x}_i$, $\boldsymbol{\omega}$) information is a structural metric of each atom's flexibility, beyond the previous classification approach defining "softness" (or "quench-in softness") as the distance to the separation plane in hyperspace [58] (or estimate of class probability [59]). Fifth, while a simple and single quantity, the resultant *SF* is shown to be indeed indicative of "structure" in terms of its behavior, i.e., its degree of responsiveness. Strong correlations with a variety of (microscopic and macroscopic) properties have been systematically demonstrated, particularly those not involved in the ML training process, including both stress-driven and thermally activated relaxation events. That is, we have achieved a wider range of utility with just one ML model, enabling the correlation of *SF* with at least five different properties. Sixth and finally, the same weighting function (vector $\boldsymbol{\omega}$ in multi-dimensional space) is found applicable for Cu–Zr MGs with different compositions and processing history. The same machine-learned bridge remains effective as the avenue to various correlations throughout a MG alloy system. The *SF* can then be evaluated from purely structural information only, requiring no further learning or relearning when the structure changes upon processing or deformation. This is therefore a useful step towards structure–property relations with minimized non-structural input (note that the latter can be either impossible to acquire, or computationally too expensive). These six merits, taken together, have gone a long way in answering the call earlier, i.e., the directive to bridge the structure on the scale and scope of local PDF with all the key properties. For instance, one can now use the magnitude of *SF* to gauge if the changes processed into the static structure would improve the MG towards desired properties, such as higher plasticity and fracture toughness.

Methods

Sample preparation

Binary Cu_xZr_{100-x} MG models with different sample sizes at different compositions were constructed through classical molecular dynamic (MD) simulation [77], with an optimized embedded atom method (EAM) potential, adopted from Ref. [78], as implemented in LAMMPS [79]. The largest time step used in this study is 2 fs. After adequate equilibration at 2500 K, the liquids of those samples were quenched to 50 K in the NPT ensemble using a Nose–Hoover thermostat with zero external pressure. The periodic boundary condition was applied in all three directions. In this work, to save computation time, some samples were first quenched to 1500 K at a rate of 1×10^{13} K/s, followed by 1×10^{12} K/s to 1000 K, then at the desired rate (effective cooling rate, in the text) to 500 K, and finally at 1×10^{13} to 50 K. This cooling schedule was verified not to cause noticeable difference in properties. All samples were equilibrated for 2 ns at 50 K before calculations of various properties. All atomic coordinates used in structure analysis are extracted from inherent structure obtained via energy minimization with conjugate gradient (CG) algorithm. Voronoi tessellation analysis [78] was employed to obtain atomic volume, and global shear modulus G was calculated using the fluctuation method [80].

Calculation of vibrational MSD

Each sample was kept in equilibrium under a microcanonical ensemble (NVE) at 50 K to calculate the vibrational MSD. The MSD of atom i is defined as $\langle (x_i(t) - \overline{x}_i)^2 \rangle$, where $\overline{x}_i$ is the equilibrium position of atom i. The MSD was computed on short time scales when the MSD is flat with time, and contains the vibrational but not the diffusional contribution. To reduce the influence from thermal fluctuation, the calculated MSD was averaged over 100 independent runs, all starting from the same configuration but with momenta assigned randomly from the appropriate Maxwell–Boltzmann distribution [81,82].

Machine learning

In all ML tasks, we treat Cu and Zr separately as two species having different favorite local packing [28]. Both classification and regression were performed, executed in LIBLINEAR package [64]. In the classification task that separates out atoms with extremely small $v_{flex,i}$ from other atoms in $Cu_{50}Zr_{50}$ MGs, the training and testing data sets were selected from Cu (Zr) atoms with the lowest 0.36% (0.18%) $v_{flex,i}$ in 150 $Cu_{50}Zr_{50}$ MGs, each containing 32,000 atoms and quenched at effective cooling rate of 1×10^{10} K/s. These inflexible atoms were label as $y_i = -1$. The same number of Cu (Zr) atoms randomly selected from the remaining atoms were labeled as $y_i = +1$. The ratio of instance number, of training set to testing set, is 4:1.

For the regression task, two different types of datasets were used. The first type contained a total of 1.35 million Cu (or Zr) atoms, i.e., 150,000 Cu (or Zr) atoms from each of 9 Cu_xZr_{100-x} samples ($x = 30, 35, \ldots, 70$, in step of 5). The nine MGs each contained 500,000 atoms and was quenched at an effective cooling rate of 1×10^{10} K/s. The second type used individual composition, and all Cu (Zr) atoms in the sample (each totaling 500,000 atoms) were used to construct the corresponding training and testing data sets at that composition. In addition, one very large dataset for $Cu_{50}Zr_{50}$ was constructed, using all Cu (Zr) atoms in 150 $Cu_{50}Zr_{50}$ MGs (each containing 32,000 atoms and quenched at an effective cooling rate of 1×10^{10} K/s); the purpose is to confirm that the models trained on those smaller data sets are reliable and the ML model trained on this single composition has similar power to that trained on the data set composed of atoms from 9 various compositions. The comparison confirmed that the ML model trained on this single composition can be transferred to other compositions in the same MG system. For all regression tasks, the ratio of instance number in training and testing data sets is 4:1. We used the natural logarithm of $v_{flex,i}$ as the target value in ML, i.e. $y_i = \ln(v_{flex,i})$, which is close to a normal distribution, as shown in Fig. S26b. This is because the distribution of $v_{flex,i}$ is rather heterogeneous, see the very long tail in Fig. S26a. To avoid high-bias or underfitting, we tuned carefully the hyperparameters in ML models, including regularization parameters, sensitiveness of the loss

function, tolerance of termination criterion, and both $\overline{r_c}$ and σ in Eq. (5) used to compute input attributes ($G(\overline{r_c})$).

Calculation of participation fraction p in soft modes

The normal mode analysis of the glass was carried out by diagonalizing the dynamical matrix of the MG inherent structure obtained using the conjugate-gradient (CG) method. The participation fraction of atom i in eigenmode e_ω is defined by $p_i = \left|\overrightarrow{e}^i_\omega\right|^2$, where $\overrightarrow{e}^i_\omega$ is the corresponding polarization vector of atom i [83]. Here, p_i was summed over a small fraction of 1% (same as that in Ref. [45]) of the lowest-frequency normal modes and denoted as the participation fraction p_i for atom i, which measures the involvement in soft modes for that atom.

Energy barrier of thermally activated events

The local potential energy landscape (PEL) was explored using ART nouveau [12,50,75,76]. For the local excitations, initial perturbations in ART were introduced by applying random displacement on a central atoms and its nearest-neighbors. The magnitude of the displacement was fixed at 0.5 Å, while the direction was randomly chosen. When the curvature of the PEL was found to be <-0.01 eV/Å^2, the system was pushed towards the saddle point using the Lanczos algorithm [84]. The saddle point is considered to be found when the overall force of the total system is below 0.05 eV/Å. The corresponding activation energy is thus the difference between the saddle point energy and the initial state energy. For each central atom in each sample, 30 relaxation events were searched.

Calculation of the velocity auto-correlation function

The velocity auto-correlation function (VACF) describes the correlation of atomic motions in the time evolution of a system. This function is defined as [85]: $\Psi(t) = \langle \overline{v}_i(\tau + t) \cdot \overline{v}_i(t) \rangle / \langle \overline{v}_i(t) \cdot \overline{v}_i(t) \rangle$, where $\overline{v}_i(t)$ is the velocity of atom i, τ is the time origin, and the angular brackets represent the ensemble average. For the samples each containing ~30,000 atoms, the same initial configuration was assigned with 100 different initial velocity fields to reduce thermal noise. For the large sample containing 1,024,000 atoms, we assigned 60 different initial velocity fields to the same initial configurations to calculate VACF for the entire sample and each group of atoms. As an example, Fig. S27 shows the VACF at 50 K of the whole $Cu_{50}Zr_{50}$ MG (containing 1,024,000 atoms and quenched at effective cooling rate of 1×10^{10} K/s).

Fictive temperature

The fictive temperature (T_f) was determined from the evolution of volume with temperature during heating at a constant rate of 1×10^{10} K/s. The fictive temperature is the temperature where the volume intersects the equilibrium liquid line when extrapolated along the glass line [48]. Fig. S28 shows an example.

Calculation of local elastic moduli

Local moduli of MGs were evaluated at 50 K using the fluctuation method as described in detail in Ref. [53]. For a canonical (*NVT*) ensemble, the local moduli can be calculated as the sum of three contributions, the fluctuation, kinetic contribution and the Born term, respectively. To reduce the statistical error in our simulated samples, the average local moduli were averaged over 20 different thermal initialization.

Data availability

The data that support the findings of this study are available from the corresponding author on request.

Author contributions

Z.F. and E.M. designed the research and led the writing of the paper. Z.F. carried out the MD simulations and machine learning. J.D. calculated the local elastic moduli. All authors contributed to data analysis and the discussions.

Acknowledgments

The authors thank C.J. Lin for useful discussions on the use of LIBLINEAR package, B. Xu for sharing the ART nouveau code, Q. Wang for sharing the code for computing interstices distribution, A. J. Liu, E. D. Cubuk, S. S. Schoenholz, and F. P. Landes for discussions on "softness", and Qi Wang and Qing-Jie Li for comments on the manuscript. The work at JHU is supported by U. S. Department of Energy (DOE) DOE-BES-DMSE under grant DE-FG02-19ER46056. This research used resources of the National Energy Research Scientific Computing Center (NERSC), a DOE Office of Science User Facility supported by the Office of Science of the U.S. Department of Energy under Contract No. DE-AC02-05CH11231, and the Maryland Advanced Research Computing Center (MARCC). J. D. acknowledges the Chinese 1000-Youth-Talent Program, and the Young Talent Startup Program of Xi'an Jiaotong University.

Appendix A. Supplementary data

Supplementary data to this article can be found online at https://doi.org/10.1016/j.mattod.2020.05.021.

References

[1] W.D. Callister Jr., Materials Science and Engineering: An Introduction, 7th ed., 2006.
[2] J. Hirth, J. Lothe, Theory of Dislocations, John Wiley & Sons, 1982.
[3] Taylor Geoffrey Ingram, H. Quinney, Proc. R. Soc. London. Ser. A, Math. Phys. Character 143 (1934) 307–326.
[4] E.O. Hall, Proc. Phys. Soc. B 64 (1951) 747–753.
[5] N.J. Petch, J. Iron Steel Inst. 174 (1953) 25–28.
[6] D.J. Safarik, R.B. Schwarz, Acta Mater. 55 (2007) 5736–5746.
[7] H. Wagner et al., Nat. Mater. 10 (2011) 439–442.
[8] Y.H. Liu et al., Phys. Rev. Lett. 106 (2011) 125504.
[9] Y. Shi, M.L. Falk, Phys. Rev. Lett. 95 (2005) 095502.
[10] Y. Shi, M.L. Falk, Phys. Rev. B 73 (2006) 214201.
[11] M.L. Manning, A.J. Liu, Phys. Rev. Lett. 107 (2011) 108302.
[12] Y. Fan, T. Iwashita, T. Egami, Nat. Commun. 5 (2014) 5083.
[13] E.D. Cubuk et al., Phys. Rev. Lett. 114 (2015) 108001.
[14] E.D. Cubuk et al., Science 358 (2017) 1033–1037.
[15] Y.Q. Cheng, J. Ding, E. Ma, Mater. Res. Lett. 1 (2013) 3–12.
[16] E. Ma, Nat. Mater. 14 (2015) 547–552.
[17] E. Ma, J. Ding, Mater. Today 19 (2016) 568–579.
[18] W.L. Johnson, MRS Bull. 24 (1999) 42–56.
[19] A.L. Greer, Science 267 (1995) 1947–1953.
[20] W.H. Wang, C. Dong, C.H. Shek, Mater. Sci. Eng.: R: Rep. 44 (2004) 45–89.
[21] J. Schroers, Phys. Today 66 (2013) 32.
[22] A.L. Greer, E. Ma, MRS Bull. 32 (2007) 611–619.
[23] A.L. Greer, Y.Q. Cheng, E. Ma, Mater. Sci. Eng.: R: Rep. 74 (2013) 71–132.
[24] C.A. Schuh, T.C. Hufnagel, U. Ramamurty, Acta Mater. 55 (2007) 4067–4109.
[25] W.L. Johnson, K. Samwer, Phys. Rev. Lett. 95 (2005) 195501.

[26] J. Zylberg et al., PNAS 114 (2017) 7289–7294.
[27] F. Spaepen, Acta Metall. 25 (1977) 407–415.
[28] Y.Q. Cheng, E. Ma, Prog. Mater Sci. 56 (2011) 379–473.
[29] J. Ding, E. Ma, NPJ Comput. Mater. 3 (2017) 9.
[30] M. Chen, Annu. Rev. Mater. Res. 38 (2008) 445–469.
[31] T.C. Hufnagel, C.A. Schuh, M.L. Falk, Acta Mater. 109 (2016) 375–393.
[32] A.S. Argon, Acta Metall. 27 (1979) 47–58.
[33] M.L. Falk, J.S. Langer, Phys. Rev. E 57 (1998) 7192–7205.
[34] D. Pan et al., PNAS 105 (2008) 14769–14772.
[35] F. Zhu et al., Nat. Commun. 7 (2016) 11516.
[36] F. Zhu et al., Phys. Rev. Lett. 119 (2017) 215501.
[37] F. Zhu et al., Nat. Commun. 9 (2018) 3965.
[38] D. Rodney, A. Tanguy, D. Vandembroucq, Modell. Simul. Mater. Sci. Eng. 19 (2011) 083001.
[39] E.F. Oleinik, M.A. Mazo, M.I. Kotelyanskii, S.N. Rudnev, O.B. Salamatina, in: Problems of Nonlinear Mechanics and Physics of Materials, Springer International Publishing, Cham, 2019, pp. 313–332.
[40] D. Srolovitz et al., Philos. Mag. A 44 (1981) 847–866.
[41] T. Egami, Prog. Mater Sci. 56 (2011) 637–653.
[42] M.D. Demetriou et al., Phys. Rev. Lett. 97 (2006) 065502.
[43] W.L. Johnson et al., MRS Bull. 32 (2007) 644–650.
[44] M. Tsamados et al., Phys. Rev. E 80 (2009) 026112.
[45] J. Ding et al., PNAS 111 (2014) 14052–14056.
[46] S. Patinet, D. Vandembroucq, M.L. Falk, Phys. Rev. Lett. 117 (2016) 045501.
[47] A. Barbot et al., Phys. Rev. E 97 (2018) 033001.
[48] P. Badrinarayanan et al., J. Non-Cryst. Solids 353 (2007) 2603–2612.
[49] J. Ketkaew et al., Nat. Commun. 9 (2018) 3271.
[50] B. Xu et al., Phys. Rev. Lett. 120 (2018) 125503.
[51] C. Liu, P. Guan, Y. Fan, Acta Mater. 161 (2018) 295–301.
[52] M.H. Cohen, G.S. Grest, Phys. Rev. B 20 (1979) 1077–1098.
[53] J. Ding, Y.-Q. Cheng, E. Ma, Acta Mater. 69 (2014) 343–354.
[54] H.L. Peng, M.Z. Li, W.H. Wang, Phys. Rev. Lett. 106 (2011) 135503.
[55] C.-X. Peng et al., Phys. Rev. B 96 (2017) 174112.
[56] P.J. Steinhardt, D.R. Nelson, M. Ronchetti, Phys. Rev. B 28 (1983) 784–805.
[57] J. Ding et al., Nat. Commun. 7 (2016) 13733.
[58] S.S. Schoenholz et al., Nat. Phys. 12 (2016) 469–471.
[59] Q. Wang, A. Jain, Nat. Commun. 10 (2019) 5537.
[60] R. Candelier et al., Phys. Rev. Lett. 105 (2010) 135702.
[61] A. Smessaert, J. Rottler, Phys. Rev. E 88 (2013) 022314.
[62] F.P. Landes et al., Phys. Rev. E 101 (2020) 010602.
[63] T. Egami, S.J.L. Billinge, Underneath the Bragg Peaks: Structural Analysis of Complex Materials, Newnes, 2012.
[64] R.-E. Fan et al., J. Mach. Learn. Res. 9 (2008) 1871–1874.
[65] T.S. Grigera et al., Nature 422 (2003) 289–292.
[66] H. Shintani, H. Tanaka, Nature Mater 7 (2008) 870–877.
[67] N. Jakse, A. Nassour, A. Pasturel, Phys. Rev. B 85 (2012) 174201.
[68] T. Brink, L. Koch, K. Albe, Phys. Rev. B 94 (2016) 224203.
[69] A. Giuntoli, D. Leporini, Phys. Rev. Lett. 121 (2018) 185502.
[70] J. Yang et al., Phys. Rev. Lett. 122 (2019) 015501.
[71] M. Baggioli, A. Zaccone, Phys. Rev. Lett. 122 (2019) 145501.
[72] J. Bünz et al., Phys. Rev. Lett. 112 (2014) 135501.
[73] T. Egami, JOM 62 (2010) 70–75.
[74] Y. Gao, H. Bei, Progr. Mater. Sci. 82 (2016) 118–150.
[75] R. Malek, N. Mousseau, Phys. Rev. E 62 (2000) 7723–7728.
[76] D. Rodney, C. Schuh, Phys. Rev. Lett. 102 (2009) 235503.
[77] C.L. Brooks, J. Solut. Chem. 18 (1989) 99–99..
[78] Y.Q. Cheng, E. Ma, H.W. Sheng, Phys. Rev. Lett. 102 (2009) 245501.
[79] S. Plimpton, J. Comput. Phys. 117 (1995) 1–19.
[80] Y.Q. Cheng, E. Ma, Phys. Rev. B 80 (2009) 064104.
[81] A. Widmer-Cooper, P. Harrowell, Phys. Rev. Lett. 93 (2004) 135701.
[82] A. Widmer-Cooper, P. Harrowell, Phys. Rev. Lett. 96 (2006) 185701.
[83] A. Widmer-Cooper et al., Nat. Phys. 4 (2008) 711–715.
[84] E. Cancès et al., J. Chem. Phys. 130 (2009) 114711.
[85] J.M. Dickey, A. Paskin, Phys. Rev. 188 (1969) 1407–1418.